# ASSESSMENT OF ANTIPLASMODIAL POTENTIAL OF *Phyllanthus amarus* ESSENTIAL OIL AND METHANOL EXTRACT WITH *In silico* PREDICTION OF PARASITE MULTISTAGE BIOACTIVE COMPOUNDS

**Onyesom, I[1*]., Ifie, E.J[2]., Acha, J.O [1]., Onuelu, J.E[3]., Enudinisu, G.N[1]. and Kilian, N[4]**

[1]Department of Medical Biochemistry, Delta State University, Abraka

[2]Faculty of Science, Valley University of Science and Technology Bushenyi, Uganda

[3]Department of Pharmacology, Delta State University, Abraka

[4]Department of Biochemistry, California State University, Chico, USA

[*]Corresponding author; Email: ionyesom@delsu.edu.ng, Orcid: 0000 0001 7095 7666

## ABSTRACT

**Background**: Malaria, predominantly caused by *Plasmodium falciparum*, remains a critical global health challenge exacerbated by increasing resistance to chloroquine and artemisinin-based combination therapies. *Phyllanthus amarus*, a medicinal plant widely used in Nigerian traditional medicine, offers promising phytochemicals for antimalarial drug development.

**Methods**: Aerial parts were extracted via hydrodistillation and Soxhlet methods to obtain essential oil (1.7% w/w) and methanol extract (6.3% w/w). Chemical profiling using GC-MS identified major constituents including γ-sitosterol and quinoline derivatives. Antiplasmodial activity was evaluated against chloroquine-sensitive (3D7) and resistant (Dd2) strains using the SYBR Green I assay, while cytotoxicity was assessed on Vero cells. *In silico* molecular docking, ADMET profiling, and density functional theory (DFT) calculations were performed on identified bioactive compounds against *Pf*DHFR, *Pf*FAS, and PfEF1-α targets.

**Results**: The essential oil demonstrated potent time-dependent inhibition ($IC_{50}$: 2.1–10.2 µg/mL at 96 h), low resistance indices (1.80–1.95), and high selectivity (SI up to 42.9). GC-MS profiling revealed 9,12,15-octadecatrien-1-ol (19.4%), 4-methoxy-3-nitrobenzyl alcohol ether (13.8%), and 8-aminoquinoline derivatives (12.5%) as major constituents in the oil, while the methanol extract contained 2′-hydroxy-6′-methoxyacetophenone acetate (15.5%) and glyoxal bis[(2,4-dinitrophenyl)hydrazone] (15.5%). *In silico* analysis identified γ-sitosterol as the most potent *Pf*DHFR binder (−9.180 kCal/mol), outperforming pyrimethamine. The quinoline derivative demonstrated strong multi-target interactions and favourable drug-like properties.

**Conclusions**: *P. amarus* extracts and their phytochemical constituents exhibit potent antiplasmodial activity, minimal cross-resistance, and multi-target potential. The quinoline derivative emerged as the most balanced lead compound, warranting further experimental validation. These findings support the development of *P. amarus*-derived compounds as novel antimalarial agents.

**Keywords**: Malaria, *Plasmodium falciparum, Phyllanthus amarus*, Chloroquine, Artemisinin, γ-Sitosterol, Molecular docking

## INTRODUCTION

Malaria remains one of the most devastating infectious diseases globally, with the WHO African Region bearing the highest burden, particularly Nigeria [1]. The escalating drug resistance exhibited by *Plasmodium falciparum* significantly contributes to this concerning trend. The 2024 World Malaria Report highlights the rapid spread of parasite resistance to available chemotherapeutic options [2]. Furthermore, conventional artemisinin combination therapies (ACTs) are expensive and often inaccessible in many local communities across Nigeria. Conversely, herbal medications are readily available, affordable, and perceived to have enhanced efficacy with reduced side effects [3].

The urgent need for novel antimalarial drugs with broad therapeutic efficacy and innovative mechanisms of action has become increasingly critical [4]. Medicinal plants represent a valuable source of such agents, with traditional knowledge guiding the discovery of bioactive compounds. Natural products offer distinct chemical scaffolds compared with synthetic drugs and can target multiple independent pathways, potentially circumventing resistance mechanisms [5].

*Phyllanthus amarus* (Euphorbiaceae), a medicinal plant widely employed in Nigerian folk medicine for treating various ailments including fever, has demonstrated promising antiplasmodial and antimalarial activities [6,7]. While, solvent extracts have been identified as active, the specific bioactive compounds in its eddential oil and their protein targets in *P. falciparum* remain incompletely characterized [8].

This study integrates experimental and computational approaches to evaluate the *in vitro* antiplasmodial activity of *P. amarus* essential oil and methanol extract against chloroquine-sensitive (3D7) and resistant (Dd2) strains, while employing *In silico* methods to predict the multistage inhibitory potential of bioactive compounds identified through GC-MS profiling.

## MATERIALS AND METHODS

### Plant Collection and Authentication

Fresh wild *P. amarus* plants were collected over one month from bushes and farmlands in Abraka, Ethiope East Local Government Area, Delta State, Nigeria. Authentication was performed by a taxonomist at the Forestry Research Institute of Nigeria (FRIN), Ibadan, Oyo State (Voucher specimen: FHI 109728). The aerial parts were washed, air-dried under shade for 30 days, and powdered for extraction.

### Extraction Procedures

*Essential Oil Extraction*: Essential oil was obtained by hydrodistillation of powdered aerial samples (500 g) using a Clevenger-type apparatus for 4 hours, following the method of Begum *et al*. [9].

*Methanol Extraction*: Methanol extract was prepared by soaking 10 g of powdered sample in 50 mL methanol for 72 hours using a Soxhlet apparatus [10].

Percentage Yield Calculation: Yield (percentage) was calculated as:

% Yield = (Weight of extract / Weight of dried plant material) × 100

**GC-MS Profiling**

Compounds in the oil and methanol extracts were identified using gas chromatography-mass spectrometry (GC-MS) analysis as previously described [10]. The GC-MS system (Agilent 7890B coupled with 5977B MSD) was equipped with an HP-5MS capillary column (30 m × 0.25 mm × 0.25 µm). Helium was used as carrier gas at a flow rate of 1 mL/min. The temperature program was: initial 50 °C (2 min), increased to 280 °C at 10 °C/min, and held for 10 min. Compound identification was performed by comparing mass spectra with NIST library databases.

***In vitro* Antiplasmodial Assay**

**Parasite culture**: Chloroquine-sensitive (*Pf*3D7) and chloroquine-resistant (*Pf*Dd2) strains of *P. falciparum* were cultured using the method of Trager and Jensen [11] with modifications. Cultures were maintained in $O^+$ human erythrocytes at 4 % hematocrit in complete RPMI 1640 medium supplemented with 0.25 % sodium bicarbonate, 0.5 % Albumax I, 45 mg/L hypoxanthine, and 50 mg/L gentamicin at 37 °C under reduced oxygen (5 % $O_2$, 5 % $CO_2$, 90 % $N_2$).

**Drug preparation**: Chloroquine stock solution (1 mM) was prepared in water. Test compounds (2.5 mg/mL) were dissolved in DMSO (0.4% v/v) and diluted in complete culture medium to achieve desired concentrations.

**Synchronization and assay**: Parasite cultures were synchronized at ring stage with 5 % sorbitol [12]. Starting parasitemias were 1 % (48 h assay), 0.25 % (72 h), or 0.1 % (96 h) with hematocrits of 1 %, 2.5 %, and 2 %, respectively. Test compounds were evaluated at concentrations of 0, 12.5, 25, 50, and 100 µg/mL. Chloroquine (100 nM for *Pf*3D7; 1 µM for *Pf*Dd2) served as positive control, while 0.5 % DMSO served as negative control.

**Fluorescence measurement**: After incubation, parasite growth was assessed using SYBR Green I fluorescence-based method [13]. Fluorescence was measured using a 96-well plate reader at excitation and emission wavelengths of 483 and 530 nm, respectively. $IC_{50}$ values were calculated by plotting mean fluorescence against drug concentration.

**Resistance index** (RI): RI was calculated as:

$RI = IC_{50}$ (*Pf*Dd2) / $IC_{50}$ (*Pf*3D7)

Higher RI values indicate greater resistance levels [14].

**Cytotoxicity Assessment**

Cytotoxicity against Vero cells was determined using the MTT assay [15]. Cells were cultured in complete RPMI containing 10 % fetal bovine serum, 0.2 % sodium bicarbonate, and 50 µg/mL gentamicin. Following 12 h incubation, test samples were added and incubated for 24 h at 37 °C in 5 % $CO_2$. MTT (5 mg/mL in PBS) was added (20 µL/well) and incubated for 3 h. Formazan crystals were dissolved in 100 µL DMSO, and absorbance was measured at 570 nm. $CC_{50}$ values were determined from dose-response curves. Selectivity Index (SI) was calculated as:

SI = $CC_{50}$ (Vero cells) / $IC_{50}$ (*Pf*3D7 or *Pf*Dd2)

SI ≥ 10 meets the "early lead" criteria for *in vitro* selectivity [16].

***In silico* Studies**

**Molecular docking**

*Ligand preparation***:** Structures of GC-MS-identified compounds were downloaded from PubChem and prepared using the LigPrep module (Schrödinger Suite 2023-4). Protonation states were adjusted to pH 7.0 using Epik, and ionization states were maintained.
*Protein preparation*: Crystal structures of target proteins (*Pf*DHFR: PDB ID 4DPD; *Pf*FAS: PDB ID 1XKT; *Pf*EF1-α: PDB ID 1F60) were obtained from the Protein Data Bank. Proteins were prepared using the Protein Preparation Wizard in Maestro. Water molecules beyond 5 Å and heteroatoms were removed, and structures were minimized to RMSD cutoff of 0.30 Å using OPLS4 force field.
*Receptor grid generation*: Grids were generated with active sites centered on bound ligand centroids using default Glide settings.
*Docking analysis:* Molecular docking was performed using Glide in extra precision (XP) mode [17]. Binding energies were evaluated using MM-GBSA approach with Prime module.

**ADMET Analysis**

Pharmacokinetic properties and drug-likeness were assessed using Lipinski's Rule of Five and Veber's rules [18]. Physicochemical characteristics, gastrointestinal absorption, blood-brain barrier permeability, and toxicity profiles were predicted using SwissADME and pkCSM web servers. Synthetic accessibility scores were evaluated using the SAscore.

**Density Functional Theory (DFT) Calculations**

Quantum chemical properties including HOMO-LUMO energies, energy gaps, chemical hardness (η), softness (δ), and electronegativity (χ) were calculated using Spartan14 software under vacuum conditions with the following equations:

$\Delta E = ELUMO - EHOMO$

$\eta = (ELUMO - EHOMO) / 2$

$\delta = 1/\eta$

$\chi = -(EHOMO + ELUMO) / 2$

**Ethical considerations**

Human erythrocytes were obtained from a certified blood bank under institutional ethical approval for laboratory use of anonymized blood products. No human participants were enrolled and no animal experiments were performed. The study complied with the principles of the Declaration of Helsinki where applicable

**Statistical Analysis**

Statistical differences between $IC_{50}$ and RI values were calculated using unpaired Student's T-test with GraphPad Prism. Z-factor was determined according to Zhang *et al*. [19], where values between 0.5 and 1.0 indicate excellent assay performance.

## RESULTS

**Extraction Yields**

The extraction yields are presented in Table 1. Methanol extraction yielded substantially higher recovery (6.3% w/w) compared with hydrodistillation (1.7% w/w), indicating a predominance of polar phytochemicals in *P. amarus*.

Table 1: Yields from the oil and methanol extract preparation from the powdered sample of the aerial parts of *Phyllanthus amarus*

| Extract | Yiled (%) |
|---|---|
| Essential oil of *P. amarus* (EOPa) | 1.7 ± 0.3 |
| Methanol extract of *P. amarus* (MEPa) | 6.3 ± 1.2 |

Data are expressed as Mean±SEM for duplicate extractions.

**GC-MS Profiling**

**Essential oil composition**: GC-MS analysis of EOPa revealed 35 compounds (Figure 1, Table 2). Major constituents included 9,12,15-octadecatrien-1-ol (Z,Z,Z) (19.405 %), 4-methoxy-3-nitrobenzyl alcohol n-pentyl ether (13.758 %), 8-amino-6-methoxy-4-methyl-5-[5-[3-trifluoromethylphenyl]pentoxy]quinol (12.530 %), and 6-amino-2-(4-methylpiperidin-1-yl)-3H-pyrimidin-4-one (9.515 %). The profile showed predominance of fatty acids, alcohols, esters, and nitrogen-containing heterocyclic compounds, with sterols including γ-sitosterol (0.123 %) and stigmasterol (0.058 %).

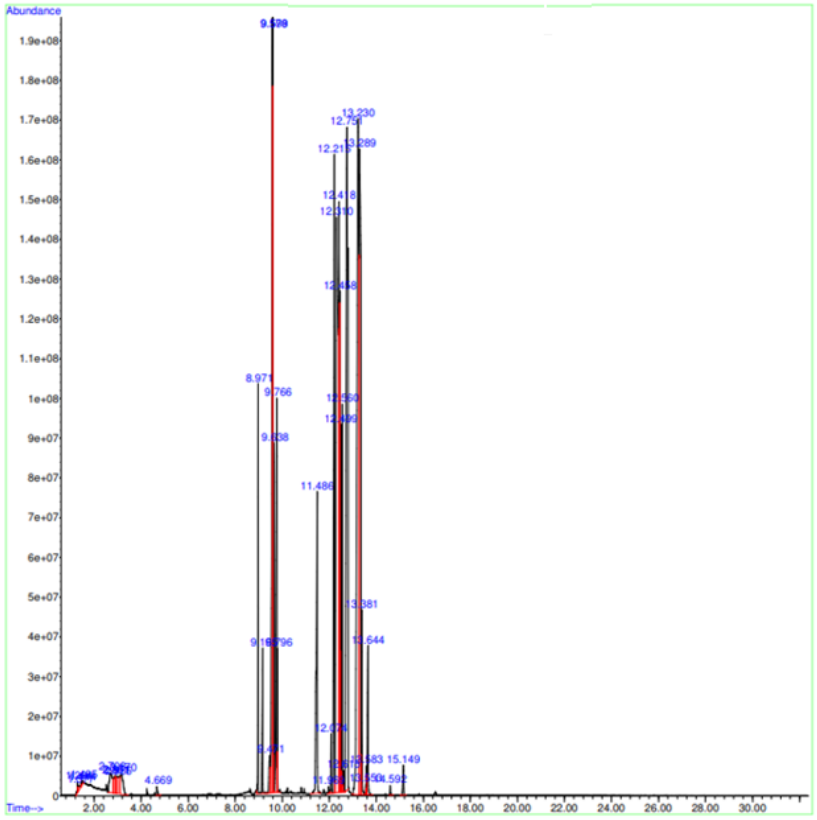


Figure 1: GC-MS spectra of essential oil *of P. amarus* (EOPa)

Table 2: GC-MS identified phytochemicals in essential oil of *P. amarus* (EOPa)

| S/N | Compound name | MW | Formula | RT (min) | Conc (%) |
|---|---|---|---|---|---|
| 1. | 1,3-Dioxonane, 5,5,6,6,7,7,8,8-octafluoro- | 274.11 | $C_7H_6F_8O_2$ | 1.376 | 0.094 |
| 2. | 1-Propanol, 2-methyl- | 74.12 | $C_4H_{10}O$ | 2.617 | 0.033 |
| 3. | 1-Pentanol | 88.15 | $C_5H_{12}O$ | 3.048 | 0.422 |
| 4. | N-hydroxy-N-methylMethanamine | 61.08 | $C_2H_7NO$ | 5.995 | 0.215 |
| 5. | Tetradecanoic acid | 228.37 | $C_{14}H_{28}O_2$ | 8.412 | 0.080 |
| 6. | D-Galactonic acid, γ-lactone | 178.14 | $C_6H_{10}O_6$ | 8.476 | 0.026 |
| 7. | 6,10,14-trimethyl2-Pentadecanone | 268.48 | $C_{18}H_{36}O$ | 8.671 | 0.142 |
| 8. | (Z)-Methyl hexadec-11-enoate | 268.44 | $C_{17}H_{32}O_2$ | 8.897 | 0.275 |
| 9. | Pentadecanoic acid, 14-methyl-, methyl ester | 270.46 | $C_{17}H_{34}O_2$ | 8.980 | 2.309 |
| 10. | n-Hexadecanoic acid | 256.43 | $C_{16}H_{32}O_2$ | 9.274 | 6.485 |
| 11. | 9,12,15-Octadecatrienoic acid, methyl ester, (Z,Z,Z)- | 292.46 | $C_{19}H_{32}O_2$ | 9.582 | 10.412 |
| 12. | 9,12,15-Octadecatrien-1-ol, (Z,Z,Z) | 264.45 | $C_{18}H_{32}O$ | 9.838 | 19.405 |
| 13. | Methyl 18-methylnonadecanoate | 326.56 | $C_{21}H_{42}O_2$ | 10.253 | 0.172 |
| 14. | Cyclododecyne | 164.29 | $C_{12}H_{20}$ | 10.339 | 0.059 |
| 15. | Eicosanoic acid | 312.54 | $C_{20}H_{40}O_2$ | 10.392 | 0.134 |
| 16. | 9,12,15-Octadecatrien-1-ol, (Z,Z,Z)- | 264.45 | $C_{18}H_{32}O$ | 10.668 | 0.048 |
| 17. | Docosanoic acid, methyl ester | 354.62 | $C_{23}H_{46}O_2$ | 10.823 | 0.205 |
| 18. | Docosanoic acid | 340.59 | $C_{22}H_{44}O_2$ | 10.961 | 0.118 |
| 19. | Tetracosanoic acid, methyl ester | 382.67 | $C_{25}H_{50}O_2$ | 11.448 | 0.131 |
| 20. | Tetracosanoic acid | 368.64 | $C_{24}H_{48}O_2$ | 11.620 | 0.031 |
| 21. | 2-Pyrazinecarboxylic acid, 3-[[[3- | 339.27 | $C_{15}H_{12}F_3N_3O_3$ | 11.791 | 0.066 |

| | | | | | |
|---|---|---|---|---|---|
| | (trifluoromethyl)phenyl]amino]carbonyl]-, ethyl ester | | | | |
| 22. | 2(3H)-Furanone, 3,4-bis(1,3-benzodioxol-5-ylmethyl)dihydro-, (3R-trans)- | 354.36 | $C_{20}H_{18}O_6$ | 12.085 | 0.379 |
| 23. | Urea, 1-[4-(chlorodifluoromethoxy)phenyl]-3-(3-methoxybenzoyl)- | 370.74 | $C_{16}H_{13}ClF_2N_2O_4$ | 12.239 | 5.229 |
| 24. | 8-Amino-6-methoxy-4-methyl-5-[5-[3-trifluoromethylphenyl]pentoxy]quinol | 418.46 | $C_{23}H_{25}F_3N_2\ O_2$ | 12.334 | 12.530 |
| 25. | dibenz[c,e][1,2]azaborine, 5,6-dihydro-7,9,10-trimethyl-6-(2,4,6-trimethylphenyl)- | 339.29 | $C_{24}H_{26}BN$ | 12.503 | 6.352 |
| 26. | Tungsten,1,2- η2-(1,3-butadiene)pentacarbonyl | 377.98 | $C_9H_6O_5W$ | 12.636 | 2.583 |
| 27. | 6-Amino-2-(4-methylpiperidin-1-yl)-3H-pyrimidin-4-one | 208.26 | $C_{10}H_{16}N_4O$ | 12.812 | 9.515 |
| 28. | 4-Methoxy-3-nitrobenzyl alcohol, n-pentyl ether | 253.30 | $C_{13}H_{19}NO_4$ | 13.306 | 13.758 |
| 29. | 3-methoxy-2,5,6-trimethylphenol | 166.22 | $C_{10}H_{14}O_2$ | 13.426 | 6.763 |
| 30. | dl-α-Tocopherol | 430.71 | $C_{29}H_{50}O_2$ | 13.623 | 0.181 |
| 31. | Benzenepropanenitrile, 3,4-dimethoxy | 191.23 | $C_{11}H_{13}NO_2$ | 13.750 | 1.430 |
| 32. | Stigmasterol | 412.69 | $C_{29}H_{48}O$ | 14.642 | 0.058 |
| 33. | γ-Sitosterol | 414.71 | $C_{29}H_{50}O$ | 15.185 | 0.123 |
| 34. | 4,22-Stigmastadiene-3-one | 410.68 | $C_{29}H_{46}O$ | 15.869 | 0.062 |
| 35. | Stigmast-4-en-3-one | 412.69 | $C_{29}H_{48}O$ | 16.586 | 0.164 |

*MW= Molecular wright, RT= Retention time, Conc.= Concentration*

**Methanol extract composition:** MEPa analysis identified 31 compounds (Figure 2, Table 3). The most abundant were 2′-hydroxy-6′-methoxyacetophenone acetate (15.534 %), glyoxal bis[(2,4-dinitrophenyl)hydrazone] (15.518 %), pentacene (6,13-diphenyl) (12.330 %), and durohydroquinone (11.063 %). Fatty acid derivatives (e.g., 9,12,15-octadecatrienoic acid methyl ester, 6.944 %) and sterols (γ-sitosterol 0.286 %; stigmasterol 0.073 %) were also present.

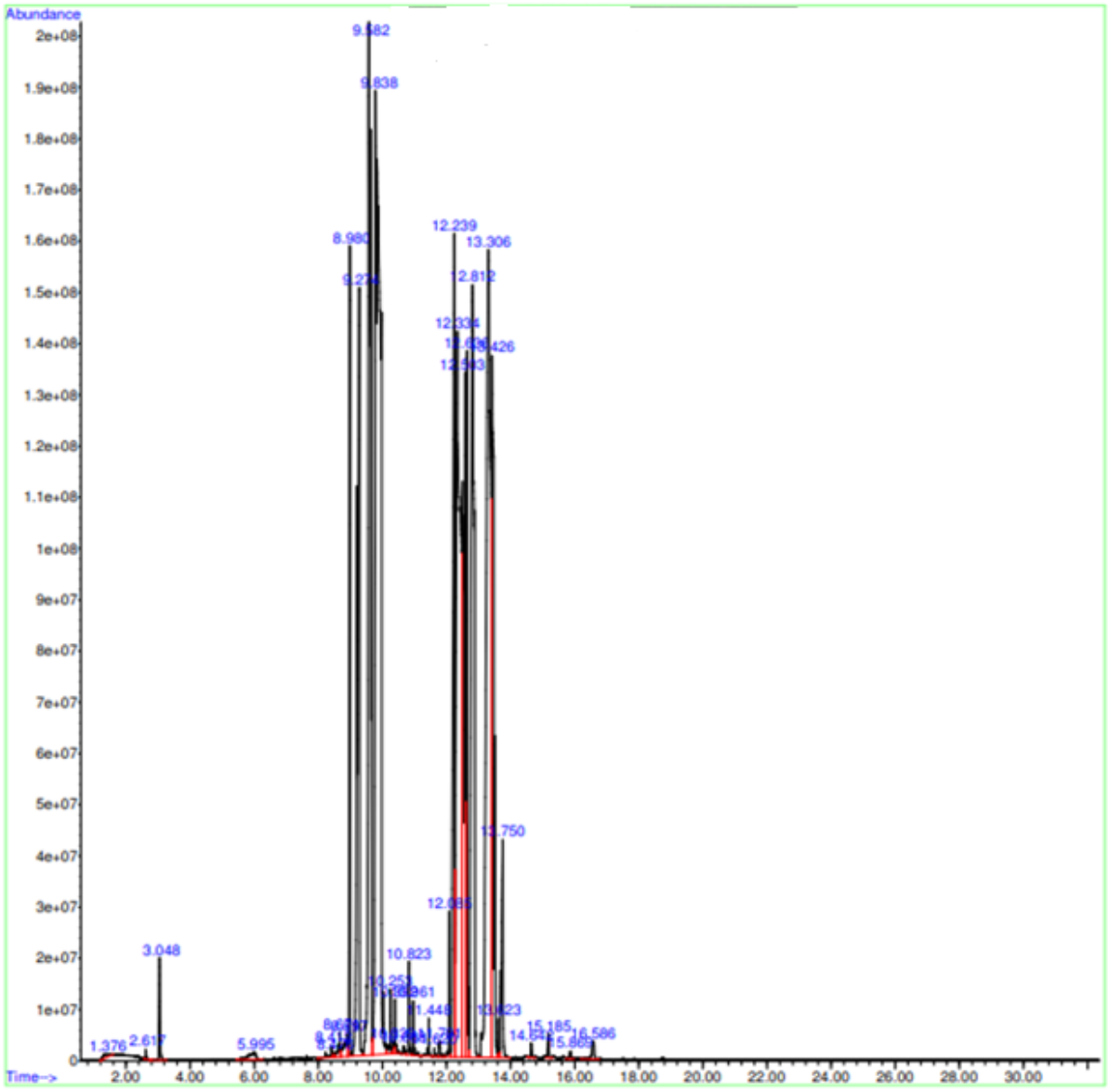


Figure 2: Spectra of the GC-MS analysis of methanol extract of *P. amarus* (MEPa)
Spectra (Figure 2) indicate thirty-one (31) phytochemicals belonging to several classes and having retention time and relative peak areas (concentration) as shown in Table 3.

Table 3: Compounds in GC-MS profile of methanol extract of *P. amarus* (MEPa)

| S/N | Compound name | MW | Formula | R.T (min) | Conc (%) |
|---|---|---|---|---|---|
| 1. | 15,24-Dimethyl-1,4,7,10,18,21-hexaoxa-15,24-diazacyclooctacosane-11,14,25,28-tetrone | 568.70 | $C_{22}H_{38}N_2O_{10}$ | 1.294 | 0.053 |
| 2. | N-Methyl-3,4-methylenedioxyamphetamine | 193.24 | $C_{11}H_{15}NO_2$ | 1.377 | 0.100 |
| 3. | 2,5,8,11-tetraoxatridecane, 13-chloro- | 242.70 | $C_9H_{19}ClO_4$ | 1.444 | 0.019 |
| 4. | Methyl chloroformate | 94.50 | $C_2H_3ClO_2$ | 1.495 | 0.052 |
| 5. | Propane, 1,1-dimethoxy-2-methyl- | 118.17 | $C_6H_{14}O_2$ | 2.708 | 0.646 |
| 6. | 2-Hexenal, 2-ethyl | 126.20 | $C_8H_{14}O$ | 4.669 | 0.085 |
| 7. | Pentadecanoic acid, 14-methyl-, methyl ester | 270.46 | $C_{17}H_{34}O_2$ | 8.971 | 1.613 |
| 8. | n-Hexadecanoic acid | 256.42 | $C_{16}H_{32}O_2$ | 9.165 | 0.889 |
| 9. | 7,10,13-Hexadecatrienoic acid, methyl ester | 264.41 | $C_{17}H_{28}O_2$ | 9.471 | 0.460 |
| 10. | 9,12,15-Octadecatrienoic acid, methyl ester, (Z,Z,Z)- | 292.46 | $C_{19}H_{32}O_2$ | 9.578 | 6.944 |
| 11. | Methyl stearate | 298.51 | $C_{19}H_{38}O_2$ | 9.638 | 1.244 |
| 12. | Octadecanoic acid | 284.48 | $C_{18}H_{36}O_2$ | 9.796 | 0.469 |
| 13. | Linolenic acid, 2-hydroxy-1-(hydroxymethyl)ethyl ester (Z,Z,Z)- | 352.51 | $C_{21}H_{36}O_4$ | 11.486 | 3.540 |
| 14. | Germacyclopentane, 1,1-diphenyl- | 268.89 | $C_{16}H_{18}Ge$ | 11.969 | 0.058 |
| 15. | 2(3H)-Furanone, 3,4-bis(1,3-benzodioxol-5-ylmethyl)dihydro-, (3R-trans)- | 354.36 | $C_{20}H_{18}O_6$ | 12.074 | 0.279 |
| 16. | 8-Amino-6-methoxy-5-[3,5-bis[trifluoromethyl]phenoxy]quinoline | 402.30 | $C_{18}H_{12}F_6N_2O_2$ | 12.215 | 5.392 |
| 17. | Glyoxal bis[(2,4-dinitrophenyl)hydrazone] | 418.28 | $C_{14}H_{10}N_8O_8$ | 12.310 | 15.518 |
| 18. | Ethanone, 2-(1H-imidazo[4,5-b]pyridin-2-yl)-1-(4-morpholyl)- | 278.33 | $C_{12}H_{14}N_4O_2S$ | 12.418 | 3.857 |
| 19. | 1(4H)-Naphthalenone, 2-[(4-cyclohexylbutyl)amino]-4-(4-methoxyphenylimino)- | 416.56 | $C_{27}H_{32}N_2O_2$ | 12.458 | 3.437 |
| 20. | Propanamide, N-(4-methylphenyl)-3-(4-phenyl-M1-piperazinyl)- | 323.44 | $C_{20}H_{25}N_3O$ | 12.499 | 2.154 |

| | | | | | |
|---|---|---|---|---|---|
| 21. | Tungsten,1,2-η2-(1,3-butadiene)pentacarbonyl- | 377.98 | $C_9H_6O_5W$ | 12.560 | 2.379 |
| 22. | 2,3,4,5-Tetrahydro-2-methyl-6-(2-(5-nitro-2-furyl)vinyl)-5-oxo-3-thioxo-1,2,4-triazine | 280.26 | $C_{10}H_8N_4O_4S$ | 12.615 | 0.158 |
| 23. | pentacene, 6,13-diphenyl- | 430.55 | $C_{34}H_{22}$ | 12.751 | 12.330 |
| 24. | 2'-Hydroxy-6'-methoxyacetophenone, acetate | 208.21 | $C_{11}H_{12}O_4$ | 13.230 | 15.534 |
| 25. | Durohydroquinone | 166.22 | $C_{10}H_{14}O_2$ | 13.289 | 11.063 |
| 26. | 1-(7-Methoxy-benzo[1,3]dioxol-5-ylmethyl)-4-(3-methyl-benzyl)-piperazine | 354.45 | $C_{21}H_{26}N_2O_3$ | 13.381 | 1.154 |
| 27. | Vitamin E | 430.71 | $C_{29}H_{50}O_2$ | 13.553 | 0.063 |
| 28. | 2(3H)-Furanone, 3,4-bis(1,3-benzodioxol-5-ylmethyl)dihydro-, (3R-trans)- | 354.36 | $C_{20}H_{18}O_6$ | 13.583 | 0.152 |
| 29. | Benzenepropanenitrile, 3,4-dimethoxy- | 191.23 | $C_{11}H_{13}NO_2$ | 13.644 | 1.224 |
| 30. | Stigmasterol | 412.69 | $C_{29}H_{48}O$ | 14.592 | 0.073 |
| 31. | γ-Sitosterol | 414.71 | $C_{29}H_{50}O$ | 15.149 | 0.286 |

*MW= Molecular weight, RT= Retention time, Conc.= Concentration*

***In vitro* Antiplasmodial Activity**

**Potency and Time-Dependent Activity**: Both extracts demonstrated time-dependent antiplasmodial activity with $IC_{50}$ values decreasing from 48 h to 96 h (Table 4). EOPa consistently outperformed MEPa across all time points and strains. Against 3D7, EOPa $IC_{50}$ values decreased from 5.5 ± 0.6 µg/mL (48 h) to 2.1 ± 0.3 µg/mL (96 h), while MEPa decreased from 8.2 ± 1.0 to 4.0 ± 0.5 µg/mL. Similar patterns were observed against Dd2 (EOPa: 10.2 ± 1.2 to 4.1 ± 0.5 µg/mL; MEPa: 15.8 ± 1.8 to 7.2 ± 0.9 µg/mL).

**Antiplasmodial action**: The ratio of $IC_{50}$ at 48 h to 96 h (<10) indicated fast-acting schizonticidal effects for both extracts against both strains (EOPa: 2.62 for 3D7, 2.49 for Dd2; MEPa: 2.05 for 3D7, 2.19 for Dd2).

**Resistance indices**: Low resistance indices (RI = 1.80–1.95) were observed for both extracts at 96 h, substantially lower than chloroquine (RI = 6.67), indicating minimal cross-resistance.

**Cytotoxicity and Selectivity**: EOPa showed lower cytotoxicity ($CC_{50}$ = 90 ± 10 µg/mL) compared with MEPa ($CC_{50}$ = 70 ± 8 µg/mL). Selectivity indices at 96 h were superior for EOPa (SI = 42.9 against 3D7; 22.0 against Dd2) compared to MEPa (SI = 17.5 against 3D7; 9.7 against Dd2). EOPa met the "early lead" criterion (SI ≥ 10) against both strains.

Table 4: Measures of antiplasmodial activity of *P. amarus* essential oil and methanol extract

| Parameter | EOPa (48 h) | EOPa (96 h) | MEPa (48 h) | MEPa (96 h) | CQ (96 h) | Notes |
|---|---|---|---|---|---|---|
| $IC_{50}$ 3D7 (µg/mL) | 5.5 ± 0.6 | 2.1 ± 0.3 | 8.2 ± 1.0 | 4.0 ± 0.5 | 0.0012 | Time-dependent activity |
| $IC_{50}$ Dd2 (µg/mL) | 10.2 ± 1.2 | 4.1 ± 0.5 | 15.8 ± 1.8 | 7.2 ± 0.9 | 0.014 | — |
| Resistance Index (RI, 96 h) | — | 1.95 | — | 1.80 | 6.67 | Low cross-resistance |
| Selectivity Index (SI, 3D7, 96 h) | — | 42.9 | — | 17.5 | — | SI ≥ 10 considered desirable |
| $CC_{50}$ Vero (µg/mL) | 90 ± 10 | 90 ± 10 | 70 ± 8 | 70 ± 8 | — | Moderate cytotoxicity |

*Values are expressed as Mean ± SEM (n = 3). EOPa = Phyllanthus amarus essential oil; MEPa = Phyllanthus amarus methanol extract; CQ = Chloroquine; RI = Resistance index ($IC_{50}$ Dd2/$IC_{50}$ 3D7); SI = Selectivity index ($CC_{50}/IC_{50}$); $CC_{50}$ = Concentration causing 50 % reduction in Vero cell viability; $IC_{50}$ = Concentration causing 50 % inhibition of Plasmodium falciparum growth.*

***In silico* Analysis**

**Molecular Docking**: Docking results against three *P. falciparum* targets are summarized in Table 5. γ-Sitosterol exhibited the strongest binding affinity to *Pf*DHFR (dock score: −9.180 kcal/mol; MM-GBSA: −62.75 kcal/mol), outperforming pyrimethamine (dock score: −7.422 kcal/mol; MM-GBSA: −55.32 kcal/mol). The quinoline derivative (8-amino-6-methoxy-4-methyl-5-[5-[3-trifluoromethylphenyl]pentoxy]quinol) showed superior docking scores against *Pf*FAS (−6.859 kcal/mol) and *Pf*EF1-α (−4.019 kcal/mol) compared to standard inhibitors (cerulenin: −3.069 kcal/mol; didemnin B: −3.553 kcal/mol). Glyoxal bis[(2,4-dinitrophenyl)hydrazone] demonstrated excellent MM-GBSA binding energies against *Pf*EF1-α (−46.05 kcal/mol).

Table 5: Docking data for the most activie compounds against each *P. falciparum* protein target

| Target | Docking Values (kCal/mol) | | |
|---|---|---|---|
| 1. *Pf*DHFR (PDB ID: 4DPD) | Dock-score | XP-Score | MMGBSA |
| • γ-Sitosterol (EOPA & MEPa) | -9.180 | -9.180 | -62.75 |
| • 8-Amino-6-methoxy-4-methyl-5-[5-[3-trifluoromethylphenyl]pentoxy]quinol (EOPa) | -7.696 | -7.696 | -53.75 |
| • Pyrimethamine (Standard inhibitor) | -7.422 | -7.911 | -55.32 |
| 2. *Pf*FAS (PDB ID: 1xkt) | | | |

| | | | |
|---|---|---|---|
| • 8-Amino-6-methoxy-4-methyl-5-[5-[3-trifluoromethylphenyl]pentoxy]quinol (EOPa) | -6.859 | -6.859 | -45.68 |
| • Glyoxal bis[(2,4-dinitrophenyl)hydrazone] (MEPa) | -4.144 | -4.144 | -46.12 |
| • Cerulenin (Standard inhibitor) | -3.069 | -3.069 | -29.68 |
| 3. *Pf*EF1-α (PDB ID:1f60) | | | |
| • 8-Amino-6-methoxy-4-methyl-5-[5-[3-trifluoromethylphenyl]pentoxy]quinol (EOPa) | -4.019 | -4.019 | -25.02 |
| • Glyoxal bis[(2,4-dinitrophenyl)hydrazone] (MEPa) | -4.019 | -4.019 | -46.05 |
| • Didemin B (Standard inhibitor) | -3.553 | -4.862 | -34.13 |

*Pf*DHFR (PDB ID: 4DPD): γ-Sitosterol exhibited the strongest binding affinity and most favourable MM/GBSA energy to *Pf*DHFR, outperforming the standard inhibitor, Pyrimethamine.
*Pf*FAS (PDB ID: 1xkt): Both 8-Amino-6-methoxy-4-methyl-5-[5-[3-trifluoromethylphenyl]pentoxy]quinol and Glyoxal bis[(2,4-dinitrophenyl)hydrazone], showed superior docking scores and binding free energies against *Pf*FAS compared with the standard inhibitor, Cerulenin.
*Pf*EF1-α (PDB ID: 1f60): Again the two compounds; 8-Amino-6-methoxy-4-methyl-5-[5-[3-trifluoromethylphenyl]pentoxy]quinol and Glyoxal bis[(2,4-dinitrophenyl)hydrazone], displayed better docking performance than the standard inhibitor, Didemnin B, with Glyoxal bis[(2,4-dinitrophenyl)hydrazone] recording the most favourable MM/GBSA binding energy.

**2D Interaction Analysis**: Binding interactions (Figures 3-5) revealed that γ-sitosterol interacts with *Pf*DHFR primarily through hydrophobic interactions and van der Waals forces. The quinoline derivative demonstrated π-π stacking and hydrophobic contacts with *Pf*DHFR. Glyoxal derivative formed multiple hydrogen bonds and electrostatic interactions with *Pf*FAS. Didemnin B exhibited extensive hydrogen bonding and hydrophobic interactions with *Pf*EF1-α.
The 2D complex interactions of the most active compounds and respective standards against each target are shown in Figures 3-5

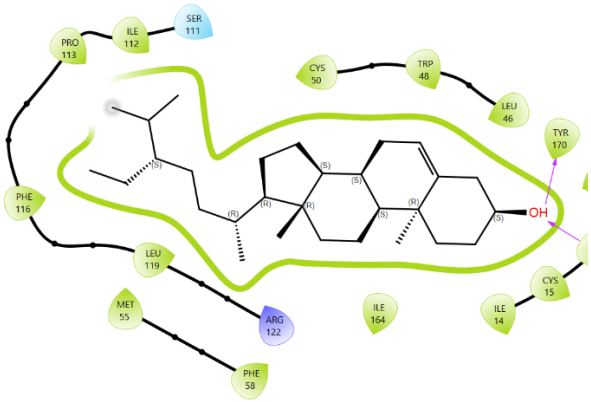


1. γ-Sitosterol in complex with *Pf*DHFR

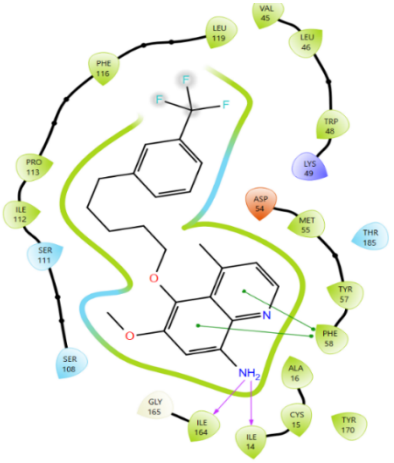


b. 8-Amino-6-methoxy-4-methyl-5-[5-[3-trifluoromethylphenyl]pentoxy]quinol in complex with *Pf*DHFR

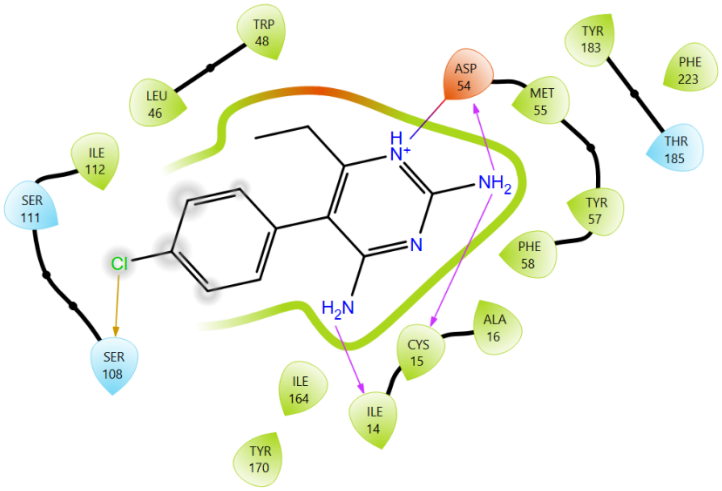


c. Pyrimethamine in complex with *Pf*DHFR

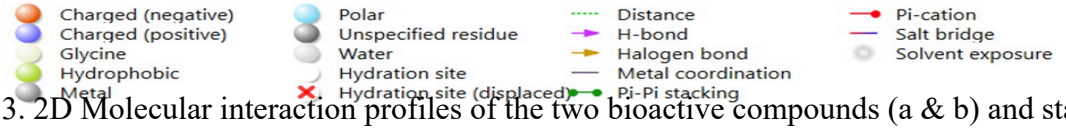


Figure 3. 2D Molecular interaction profiles of the two bioactive compounds (a & b) and standard, Pyrimethamine (c) with *Pf*DHFR

The binding interactions show that both γ-sitosterol and the quinol derivative interact with the active site of *Pf*DHFR mainly through hydrophobic interactions and van der Waals forces, with limited hydrogen bonding compared to the standard drug pyrimethamine. Pyrimethamine exhibits stronger and more specific hydrogen bond interactions with key amino acid residues, explaining its higher binding specificity. The quinol compound, however, demonstrates moderate binding through a combination of π-π stacking and hydrophobic contacts, suggesting potential inhibitory activity.

Acta Biomed 2026; Vol. 97, N. 1: ISSN: 0392-4203 | eISSN: 2531-6745

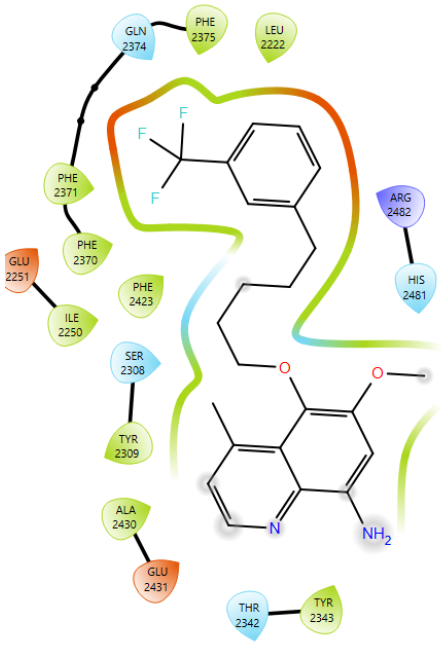


a. 8-Amino-6-methoxy-4-methyl-5-[5-[3-trifluoromethy
Fatty Acid Synthase (FAS).

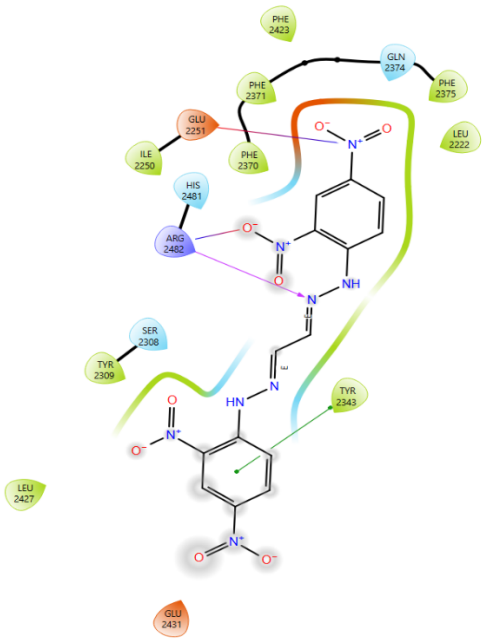


b. Glyoxal bis[(2,4-dinitrophenyl)hydrazone] in complex with FAS

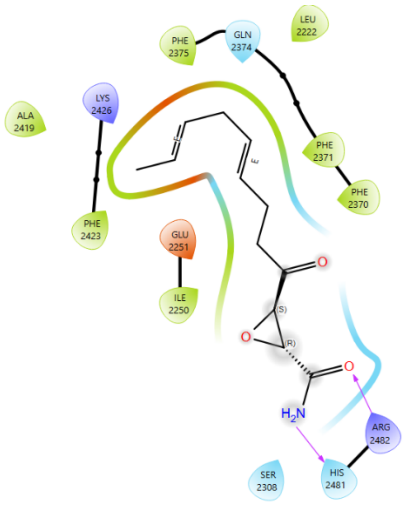


c. Cerulenin in complex with FAS

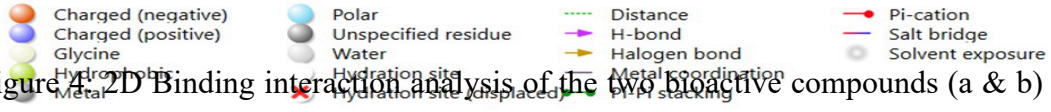


Figure 4. 2D Binding interaction analysis of the two bioactive compounds (a & b) and standard, Cerulenin (c) with *P. falciparum* Fatty Acid Synthase (*Pf*FAS)

In *Pf*FAS binding, the glyoxal derivative shows strong interaction characterized by multiple hydrogen bonds and electrostatic interactions, indicating a stable ligand–protein complex. The quinol compound displays mixed interactions including hydrophobic and weak polar contacts, while the standard cerulenin forms well-defined binding through covalent-like and hydrophobic

Acta Biomed 2026; Vol. 97, N. 1: ISSN: 0392-4203 | eISSN: 2531-6745

interactions within the enzyme active pocket. The glyoxal compound's higher polarity enhances its binding affinity compared with others.

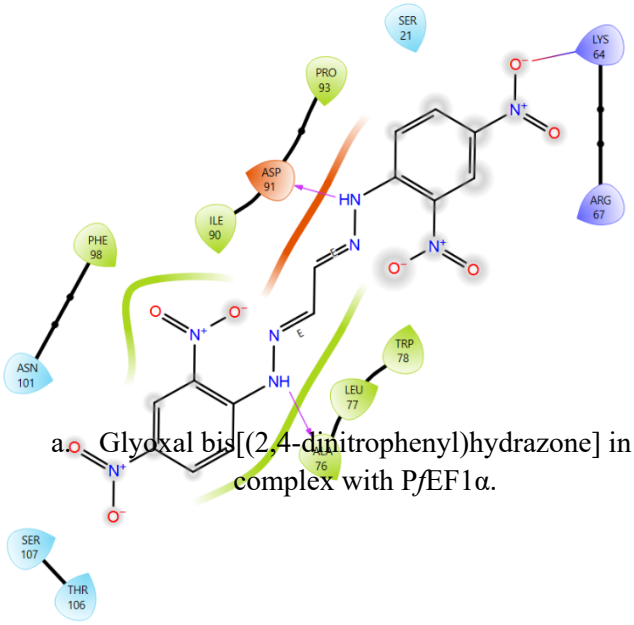


a. Glyoxal bis[(2,4-dinitrophenyl)hydrazone] in complex with P*f*EF1α.

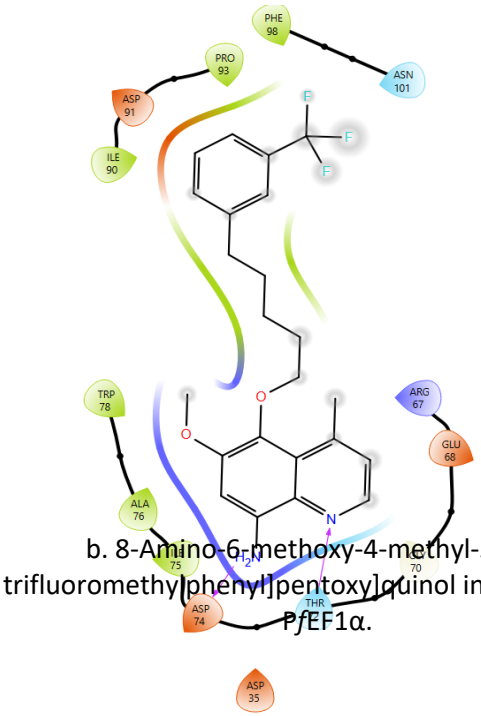


b. 8-Amino-6-methoxy-4-methyl-5-[5-[3-trifluoromethyl]phenyl]pentoxy]quinol in complex with P*f*EF1α.

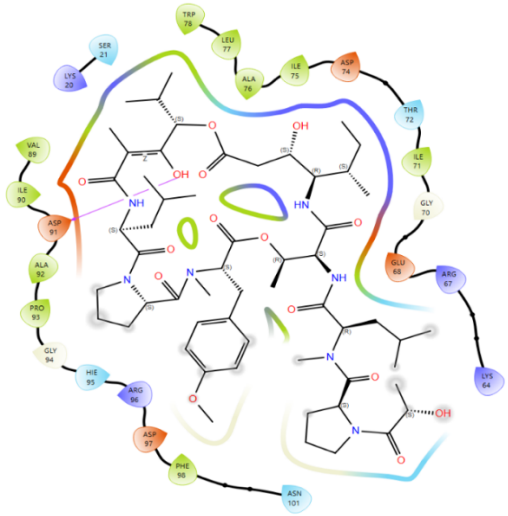

c. Didemin B in complex with *Pf*EF1α.

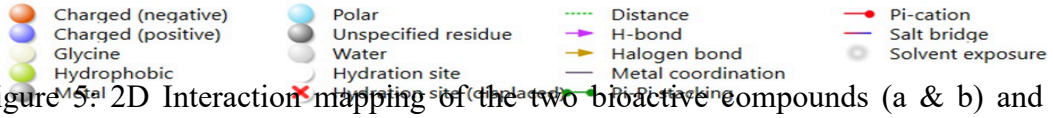


Figure 5. 2D Interaction mapping of the two bioactive compounds (a & b) and the standard, Didemin B (c) with *Plasmodium falciparum* Elongation Factor 1α (*Pf*EF1α)

For *Pf*EF1α, both glyoxal derivative and quinol compound exhibit significant binding via hydrogen bonding, π-alkyl interactions, and electrostatic forces. The glyoxal compound showed stronger interaction due to its multiple electron-withdrawing groups, enabling better interaction with amino acid residues. The standard, Didemin B, demonstrates highly stable binding through

Acta Biomed 2026; Vol. 97, N. 1: ISSN: 0392-4203 | eISSN: 2531-6745

extensive hydrogen bonding and hydrophobic interactions, serving as a benchmark for strong inhibitory potential.

**Drug-Likeness of the Bioactive Compounds**: Drug-likeness assessment (Table 6) showed that the quinoline derivative violated no Lipinski's or Veber's rules, with a bioavailability score of 0.55 and synthetic accessibility of 3.03. γ-Sitosterol violated Veber's rule (one violation) and had a synthetic accessibility score of 6.30. Glyoxal compound showed two violations (Lipinski's and Veber's).

Table 6: Drug likeness of the predicted bioactive compounds

| Drug likeness | γ-Sitosterol | 8-Amino-6-methoxy-4-methyl-5-[5-[3-trifluoromethylphenyl]pentoxy]quinol | Glyoxal bis[(2,4-dinitrophenyl)hydrazone] |
|---|---|---|---|
| Lipinski's rule | 1 | 0 | 1 |
| Veber rule | 0 | 0 | 1 |
| Bioavailability | 0.55 | 0.55 | 0.55 |
| Synthetic Accessibility | 6.30 | 3.03 | 1.85 |

γ-Sitosterol meets Verber's rule, but not Lipinski's, suggesting some limitations in bioavailability (score 0.55) with a higher synthetic accessibility score (6.30), indicating greater synthesis complexity. 8-Amino-6-methoxy-4-methyl-5-[5-[3-trifluoromethylphenyl]pentoxy]quinol has lower Lipinski's and Veber scores, reflecting more favourable drug-like properties.

**Physicochemical properties of the active compounds**

Physicochemical analysis (Table 7) revealed γ-sitosterol as the most lipophilic (fraction $Csp^3$ = 0.93, TPSA = 20.23 Å², molar refractivity = 133.23), while glyoxal compound was the most polar (TPSA = 232.06 Å², 10 H-bond acceptors). The quinoline derivative demonstrated balanced properties (TPSA = 57.37 Å², 6 H-bond acceptors).

| Property | γ-Sitosterol | 8-Amino-6-methoxy-4-methyl-5-[5-[3-trifluoromethylphenyl]pentoxy]quinol | Glyoxal bis[(2,4-dinitrophenyl)hydrazone] |
|---|---|---|---|
| Formula | $C_{29}H_{50}O$ | $C_{23}H_{25}F_3N_2O_2$ | $C_{14}H_{10}N_8O_8$ |
| Molecular Weight (MW g/mol) | 414.71 | 418.45 | 418.28 |
| Number of heavy atoms | 30 | 30 | 30 |
| Number of aromatic | 0 | 16 | 12 |

Acta Biomed 2026; Vol. 97, N. 1: ISSN: 0392-4203 | eISSN: 2531-6745

| | | | |
|---|---|---|---|
| heavy atoms | | | |
| Fraction $Csp^3$ | 0.93 | 0.35 | 0.00 |
| Number of rotatable bonds | 6 | 9 | 9 |
| Number of H-bond acceptors | 1 | 6 | 10 |
| Number of H-bond donors | 1 | 1 | 2 |
| Molar refractivity | 133.23 | 112.81 | 112.04 |
| TPSA (Å²) | 20.23 | 57.37 | 232.06 |
| Solubility | Poorly soluble | Moderately soluble | Moderately soluble |

γ-Sitosterol exhibited the most lipophilic profile (Fraction $Csp^3$ = 0.93, TPSA = 20.23 Å²) with the highest molar refractivity, favouring excellent membrane permeability despite its poor aqueous solubility. Then, 8-Amino-6-methoxy-4-methyl-5-[5-[3-trifluoromethylphenyl]pentoxy]quinol presented relatively balanced drug-like properties with moderate TPSA (57.37 Å²) and solubility, making it the most promising candidate among the three. In contrast, Glyoxal bis[(2,4-dinitrophenyl)hydrazone] was the most polar compound (TPSA = 232.06 Å², 10 H-bond acceptors), which may severely limit its membrane permeability and bioavailability.

**ADME Properties of Active Compounds**

All three compounds showed low gastrointestinal absorption and no blood-brain barrier permeation (Table 8). Toxicity profiling (Table 9) identified γ-sitosterol as the safest compound (negative for AMES, hepatotoxicity, and skin sensitization). The quinoline derivative showed moderate hepatotoxicity concerns, but was negative for mutagenicity and cardiac risks. Glyoxal compound was positive for AMES toxicity and hepatotoxicity, with extremely low maximum tolerated dose (−0.066 mg/kg/day).

Table 8: ADME characteristics of the bioactive compounds

| Compounds | GI absorption | BBB permeation |
|---|---|---|
| γ-Sitosterol | Low | No |
| 8-Amino-6-methoxy-4-methyl-5-[5-[3-trifluoromethylphenyl]pentoxy]quinol | Low | No |
| Glyoxal bis[(2,4-dinitrophenyl)hydrazone] | Low | No |

Acta Biomed 2026; Vol. 97, N. 1: ISSN: 0392-4203 | eISSN: 2531-6745

All three compounds displayed low gastrointestinal (GI) absorption and no blood-brain barrier (BBB) permeation. This profile suggests poor oral bioavailability and minimal potential for crossing into the central nervous system.

**Toxicity Profile**

Table 9: Toxicity profile of the bioactive compounds

The toxicity profile (Table 9) indicates that γ-Sitosterol demonstrated the safest toxicity profile among the three compounds, testing negative for AMES toxicity, hepatotoxicity, and skin sensitization. 8-Amino-6-methoxy-4-methyl-5-[5-[3-trifluoromethylphenyl]pentoxy]quinol showed moderate safety concerns, primarily due to predicted hepatotoxicity, but remained free from mutagenic and cardiac risks. In contrast, Glyoxal bis[(2,4-dinitrophenyl)hydrazone] displayed the most unfavourable profile, being the only compound positive for AMES toxicity, while also, exhibiting hepatotoxicity and an extremely low maximum tolerated dose (−0.066 mg/kg/day).

| | γ-Sitosterol | 8-Amino-6-methoxy-4-methyl-5-[5-[3-trifluoromethylphenyl]pentoxy]quinol | Glyoxal bis[(2,4-dinitrophenyl)hydrazone] |
|---|---|---|---|
| AMES Toxicity | No | No | Yes |
| Max. Tolerated Dose (Human) (mg/kg/day) | -0.62 | 0.04 | -0.066 |
| hERG Inhibition | No | No | No |
| LD50 | 2.55 | 2.61 | 2.709 |
| Hepatotoxicity | No | Yes | Yes |
| Skin Sensitization | No | No | No |
| *T. Pyriformis* Toxicity | 0.43 | 0.42 | 0.305 |
| Minnow Toxicity | -1.80 | -3.85 | 0.753 |

Acta Biomed 2026; Vol. 97, N. 1: ISSN: 0392-4203 | eISSN: 2531-6745

**Density Functional Theory (DFT) Analysis**

DFT calculations (Table 10, Table 11) showed that γ-sitosterol had the widest HOMO-LUMO gap (6.80 eV) and highest chemical hardness (3.40 eV), indicating greater stability and lower reactivity. Glyoxal bis[(2,4-dinitrophenyl)hydrazone] showed the narrowest gap (3.40 eV), highest softness (0.59 $eV^{-1}$), and highest electronegativity (4.90 eV), correlating with enhanced target binding. The quinoline derivative exhibited intermediate properties (gap: 3.80 eV; softness: 0.53 $eV^{-1}$; electronegativity: 2.90 eV).

Table 10: Density Functional Theory (DFT) analysis of the bioactive compounds

| Parameter | γ-Sitosterol | 8-Amino-6-methoxy-4-methyl-5-[5-[3-trifluoromethylphenyl]pentoxy]quinol | Glyoxal bis[(2,4-dinitrophenyl)hydrazone] |
|---|---|---|---|
| HOMO (eV) | -6.20 | -4.80 | -6.60 |
| LUMO (eV) | 0.60 | -1.00 | -3.20 |
| ΔE-gap (eV) | 6.80 | 3.80 | 3.40 |
| η (Hardness, eV) | 3.40 | 1.90 | 1.70 |
| δ (Softness, $eV^{-1}$) | 0.29 | 0.53 | 0.59 |
| χ (Electronegativity, eV) | 2.80 | 2.90 | 4.90 |

*HOMO: Highest Occupied Molecular Orbital, LUMO: Lowest Unoccupied Molecular Orbital, ΔE-gap: Energy difference between HOMO and LUMO, η (Hardness), δ (Softness), χ (Electronegativity).*

γ-Sitosterol has higher HOMO-LUMO energy gap (ΔE) and hardness (η), indicating that, it is more chemically stable and less reactive. Glyoxal bis[(2,4-dinitrophenyl)hydrazone] and 8-Amino-6-methoxy-4-methyl-5-[5-[3-trifluoromethylphenyl]pentoxy]quinol showed smaller gaps and lower hardness, but higher softness, indicating they are more chemically reactive and potentially better at interacting with biological targets. Electronegativity values suggest the tendency to attract electrons, with Glyoxal bis[(2,4-dinitrophenyl)hydrazone] having the highest electronegativity, which may contribute to stronger binding interactions in docking studies.

Table 11: 2D molecular structures of DFT analysis of the bioactive compounds

| Compound | HOMO | Energy gap | LUMO |
|---|---|---|---|
| γ-Sitosterol | 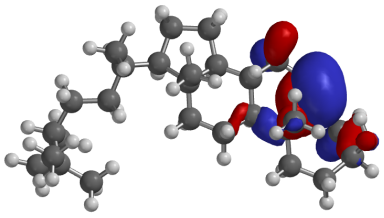 | 6.80 | 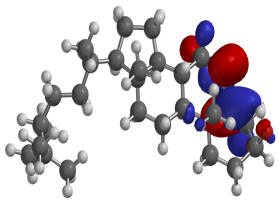 |

Acta Biomed 2026; Vol. 97, N. 1: ISSN: 0392-4203 | eISSN: 2531-6745

| | | | |
|---|---|---|---|
| 8-Amino-6-methoxy-4-methyl-5-[5-[3-trifluoromethylphenyl]pentoxy]quinol | 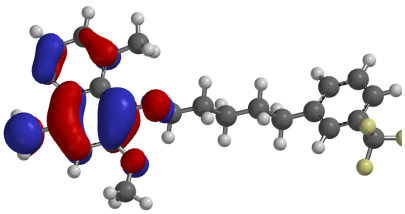 | 3.80 | 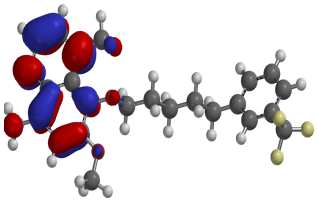 |
| Glyoxal bis[(2,4-dinitrophenyl)hydrazone] | 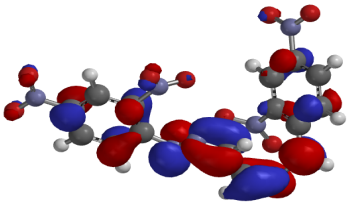 | 3.40 | 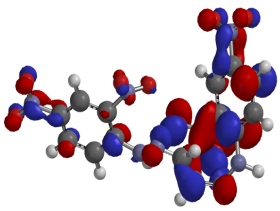 |

DFT analysis highlighted quantum chemical differences: γ-Sitosterol possessed the widest HOMO-LUMO gap (6.80 eV) and highest chemical hardness, indicating greater stability and lower reactivity. The quinoline derivative (gap 3.80 eV) and especially glyoxal compound (gap 3.40 eV, highest softness and electronegativity) displayed narrower gaps, higher softness, and stronger electron-withdrawing character, potentially explaining their favourable target interactions in docking.

## DISCUSSION

The significantly higher methanol extraction yield (6.3 %) compared with essential oil yield (1.7 %) reflects the predominance of polar phytochemicals in *P. amarus*. This finding aligns with previous studies reporting 5-15 % yields for polar solvent extractions of *Phyllanthus* species [20,21]. Methanol effectively solubilizes lignans (phyllanthin, hypophyllanthin), flavonoids, tannins, alkaloids, and phenolic acids characteristic of *P. amarus* [22], while hydrodistillation selectively isolates volatile non-polar terpenoids constituting a minor fraction of secondary metabolites.

GC-MS profiling revealed complex phytochemical compositions. The dominance of 9,12,15-octadecatrien-1-ol (linolenyl alcohol) in EOPa (19.4 %) and the abundant methyl esters of fatty acids suggest significant antioxidant and anti-inflammatory potential [23]. The identification of 8-aminoquinoline derivatives (12.5 % in EOPa; 5.4% in MEPa) is noteworthy, as quinoline moieties constitute the pharmacophore of established antimalarials including chloroquine and amodiaquine [24]. The presence of γ-sitosterol (0.123 % in EOPa; 0.286 % in MEPa) and stigmasterol, phytosterols known for membrane-stabilizing and immunomodulatory properties [25], contributes to the bioactivity profile.

In MEPa, the high abundance of 2′-hydroxy-6′-methoxyacetophenone acetate (15.5 %) and glyoxal bis[(2,4-dinitrophenyl)hydrazone] (15.5 %) suggests these compounds significantly contribute to the extract's biological activities. The presence of durohydroquinone (11.1 %), a polyphenolic

Acta Biomed 2026; Vol. 97, N. 1: ISSN: 0392-4203 | eISSN: 2531-6745

compound, reinforces antioxidant potential. The detection of nitrogen- and sulfur-containing heterocycles indicates possible antimicrobial and pharmacological relevance [26].

The essential oil demonstrated superior antiplasmodial activity compared with methanol extract across all time points and strains. This observation likely reflects the enhanced membrane permeability and target affinity of lipophilic constituents in the oil [27]. The $IC_{50}$ values (2.1–10.2 µg/mL for EOPa) compare favourably with literature reports on *P. amarus* ethanol extracts ($IC_{50}$: 5.80 µg/mL against clinical isolates) [28] and aqueous/ethanol extracts ($IC_{50}$: 10–30 µg/mL against Dd2) [29].

The time-dependent decrease in $IC_{50}$ values from 48 h to 96 h indicates a slow-acting schizonticidal effect, characteristic of many plant-derived antimalarials. The ratio of $IC_{50}$ at 48 h to 96 h (<10) confirms fast-acting action according to established criteria [30]. This kinetics pattern suggests interference with multiple stages of the intraerythrocytic developmental cycle.

The remarkably low resistance indices (RI: 1.80–1.95) demonstrate minimal cross-resistance with chloroquine, a significant advantage in endemic regions where chloroquine resistance is prevalent. The chloroquine indices (CI ≈ 293–3,333) confirm that while higher concentrations are required compared with chloroquine, the extracts retain meaningful activity against resistant parasites.

Selectivity indices of EOPa (42.9 against 3D7; 22.0 against Dd2) substantially exceed the SI ≥ 10 threshold considered promising for "early lead" candidates [16]. This compares favourably with alkaloid-rich fractions of *P. amarus* achieving SI values up to 105.67 [8]. The moderate cytotoxicity ($CC_{50}$: 70–90 µg/mL) coupled with potent antiplasmodial effects supports further development of these extracts, particularly the essential oil, for bioassay-guided fractionation and *in vivo* validation.

Molecular docking identified three compounds with promising multi-target potential: γ-sitosterol, the quinoline derivative, and glyoxal bis[(2,4-dinitrophenyl)hydrazone]. The selection of *Pf*DHFR, *Pf*FAS, and *Pf*EF1-α as targets is clinically relevant: *Pf*DHFR is a validated target for antifolate drugs [31], *Pf*FAS is essential for apicoplast-mediated fatty acid synthesis during blood-stage growth [32], and *Pf*EF1-α is critical for protein synthesis and parasite survival [33].

γ-Sitosterol's superior binding to *Pf*DHFR (−9.180 kCal/mol) compared with pyrimethamine (−7.422 kCal/mol) is remarkable, considering it is a naturally occurring phytosterol. This observation aligns with recent virtual screening studies where phytosterols achieve dock scores of −8.0 to −10.5 kcal/mol against *Pf*DHFR [34]. The favourable MM-GBSA energy (−62.75 kCal/mol) suggests thermodynamically stable complex formation, potentially explaining its *in vitro* activity against chloroquine-resistant strains.

The quinoline derivative demonstrated balanced multi-target affinity, with superior docking scores against *Pf*FAS (−6.859 kcal/mol) and *Pf*EF1-α (−4.019 kcal/mol) compared with standard inhibitors. This is consistent with the established antimalarial activity of quinoline-based scaffolds through multiple mechanisms, including haem polymerization inhibition and enzyme targeting [35]. The presence of trifluoromethyl and pentoxy substituents likely enhances binding affinity through hydrophobic interactions and electron-withdrawing effects.

Acta Biomed 2026; Vol. 97, N. 1: ISSN: 0392-4203 | eISSN: 2531-6745

Glyoxal bis[(2,4-dinitrophenyl)hydrazone] showed excellent MM-GBSA energies against *Pf*EF1-α (−46.05 kCal/mol), although its toxicity profile raises concerns. The 2D interaction analysis revealed multiple hydrogen bonds and electrostatic interactions, consistent with its high polarity and electronegativity.

The quinoline derivative emerged as the most balanced candidate based on combined docking, drug-likeness, and safety profiles. Its compliance with Lipinski's and Veber's rules, moderate TPSA (57.37 Å²), and synthetic accessibility score (3.03) indicate favourable drug-like properties and synthetic feasibility [36]. The low gastrointestinal absorption prediction for all compounds suggests challenges for oral administration, potentially necessitating formulation strategies or alternative routes.

γ-Sitosterol's high lipophilicity (TPSA: 20.23 Å², fraction $Csp^3$: 0.93) and low aqueous solubility may limit bioavailability, despite its excellent binding affinity and safety profile. Its high synthetic accessibility score (6.30) indicates synthesis complexity. However, its negative toxicity profile (negative AMES, hepatotoxicity, skin sensitization) supports consideration as a lead compound requiring derivatization to improve solubility.

The glyoxal compound's unfavourable toxicity profile (AMES positive, hepatotoxicity, extremely low tolerated dose) suggests it requires significant structural modification to mitigate safety concerns. This highlights the importance of integrating toxicity prediction early in the drug discovery pipeline.

DFT analysis revealed quantum chemical distinctions among the compounds. γ-Sitosterol's wide HOMO-LUMO gap (6.80 eV) and high chemical hardness (3.40 eV) indicate greater stability and lower reactivity, suitable for sustained molecular interactions without chemical degradation. The narrower gaps observed for the quinoline (3.80 eV) and glyoxal (3.40 eV) derivatives, coupled with higher softness (0.53 and 0.59 $eV^{-1}$, respectively), correlate with enhanced target binding propensity [37].

The high electronegativity of glyoxal compound (4.90 eV) explains its tendency for electron sharing and formation of multiple hydrogen bonds observed in docking studies. Conversely, γ-sitosterol's lower electronegativity (2.80 eV) aligns with its predominantly hydrophobic interaction profile. These quantum chemical insights provide mechanistic explanations for the binding differences observed in molecular docking and support the structure-activity relationships of these phytochemicals.

The integration of *in vitro* antiplasmodial activity with *In silico* predictions strengthens the evidence base for *P. amarus*-derived compounds as antimalarial leads. The essential oil, with its complex mixture of bioactive compounds, showed the most potent activity, likely reflecting synergistic interactions among constituents. This aligns with the traditional use of whole plant extracts in ethnomedicine, where multiple compounds collectively contribute to therapeutic effects [38].

The quinoline derivative, identified through GC-MS profiling and prioritized through computational screening, represents a promising scaffold for further optimization. Its presence in both EOPa (12.5 %) and MEPa (5.4 %) suggests it is a major bioactive constituent contributing to

the observed antiplasmodial activity. The identification of γ-sitosterol as a potent *Pf*DHFR binder provides a rationale for the activity against chloroquine-resistant strains, as it targets a distinct pathway from chloroquine.

## CONCLUSION

The essential oil and methanol extract of *P. amarus* demonstrated potent, time-dependent antiplasmodial activity against both chloroquine-sensitive and resistant *P. falciparum* strains, with the essential oil showing superior potency ($IC_{50}$: 2.1 µg/mL at 96 h), favourable resistance indices (RI: 1.80-1.95), and high selectivity (SI: 42.9). GC-MS profiling identified major bioactive constituents including 9,12,15-octadecatrien-1-ol, quinoline derivatives, and phytosterols. *In silico* analysis identified γ-sitosterol, the quinoline derivative, and glyoxal bis[(2,4-dinitrophenyl)hydrazone] as multi-target binders against *Pf*DHFR, *Pf*FAS, and *Pf*EF1-α. The quinoline derivative emerged as the most balanced lead compound based on favourable docking across targets, drug-like properties, and moderate safety profile. These findings integrate traditional knowledge with modern evidence-based approaches, supporting the development of *P. amarus*-derived compounds as novel antimalarial agents and demonstrating the value of combining experimental bioassays with computational screening for accelerated lead discovery from African medicinal flora.

**Conflict of interest**: No conflict of interest to declare

**Funding**: The research was supported by the TETFund IBR grant (TETF/DR&D/CE/UNI/ABRAKA/IBR/2021/VOL.1)

**Authors' Contributions**: OI conceptualize the research, designed and supervised the study. AJO and OJE performed the laboratory tasks, while EGN did the statistical analysis and interpreted the results. IEJ and KN organized and supervised the laboratory conduct. All authors were involved in preparing the manuscript for publication

## REFERENCES

[1] World Health Organization. Guidelines for malaria. Geneva: WHO Press; 2025.
[2] World Health Organization. World malaria report 2024. Geneva: WHO; 2025.
[3] Evbuomwan IO, Adeyemi OS, Oluba OM. Indigenous medicinal plants used in folk medicine for malaria treatment in Kwara State, Nigeria: an ethnobotanical study. BMC Complement Med Ther. 2023;23:324.
[4] White NJ. Antimalarial drug resistance. J Clin Invest. 2004;113(8):1084-92.
[5] Wells TNC. Natural products as starting points for future anti-malarial therapies: going back to our roots? Malar J. 2011;10(Suppl 1):S3.
[6] Uzuegbu UE, Opajobi AO, Utalor JE, Elu CO, Onyesom I. Cytotoxicity and antiplasmodial activity of alkaloid extracts prepared from eight African medicinal plants used in Nigeria. Thai J Pharm Sci. 2020;44(4):237-44.
[7] Opajobi AO, Ojugbeli ET, Uzuegbu UE, Elu CO, Toloyai PY, Awhin PE, Oshiegbu W, Onyesom I. Inhibition of Plasmodium berghei growth by alkaloid extract of *Phyllanthus amarus*

in mice increased haem level and stabilized erythrocyte membrane. Int J Health Sci. 2022;6(S2):13028-43.
[8] Uzuegbu UE, Onyesom I, Opajobi AO, Elu CO. Evaluation of erythrocyte viability, antioxidant capacity and antiplasmodial activity induced by alkaloid extract of *Phyllanthus amarus*. J Herbmed Pharmacol. 2022;11(4):554-61.
[9] Begum M, Lyngdoh W, Sharma HK. Formulation and evaluation of mosquito repellent ointment prepared with the essential oil of Zanthoxylum acanthopodium DC. indigenous to Northeast India. Int J Green Pharm. 2018;12(3):S518.
[10] Ameen OA, Hamid AA, Yusuf Q, Njoku OG, Oseni TO, Jamiu W. Quantitative and qualitative assessment of phytochemicals in methanolic extracts of hurricane weed (*Phyllanthus amarus* Schumach. & Thonn) plant. J Appl Sci Environ Manage. 2021;25(2):159-65.
[11] Trager W, Jensen FB. Cultivation of malaria parasite. Nature. 1978;273:621-2.
[12] Lambros C, Vanderberg JP. Synchronization of *Plasmodium falciparum* erythrocytic stages in culture. J Parasitol. 1979;65(3):418-20.
[13] Smilkstein M, Sriwilaijaroen N, Kelly JX, Wilairat P, Riscoe M. Simple and inexpensive fluorescence-based technique for high-throughput antimalarial drug screening. Antimicrob Agents Chemother. 2004;48(5):1803-6.
[14] Arnold MSJ, Wittlin S, Rottmann M, Brun R, Kaiser M. Antiplasmodial activity of the natural product compounds alstonine and himbeline. Int J Parasitol Drugs Drug Resist. 2021;16:17-22.
[15] Mosmann T. Rapid colorimetric assay for cellular growth and survival: application to proliferation and cytotoxicity assays. J Immunol Methods. 1983;65:55-63.
[16] Medicine for Malaria Venture. Information for scientists [Internet]. Geneva: MMV; 2021 [cited 2021 Nov 10]. Available from: https://www.mmv.org/research-development/information-scientists
[17] Afolayan FID, Oladokun SE. *In silico* antiplasmodial effects of phytocompounds derived from Andrographis paniculata on validated drug targets of different stages of *Plasmodium falciparum*. Infect Dis Res. 2024;5:1-12.

[18] Veber DF, Johnson SR, Cheng HY, Smith BR, Ward KW, Kopple KD. Molecular properties that influence the oral bioavailability of drug candidates. J Med Chem. 2002;45(12):2615-23.
[19] Zhang JH, Chung TD, Oldenburg KR. A simple statistical parameter for use in evaluation and validation of high throughput screening assays. J Biomol Screen. 1999;4(2):67-73.
[20] Nguyen VT, Le TT, Le TH, Nguyen TT. Physicochemical properties, antioxidant and cytotoxic activities of *Phyllanthus amarus* extracts. Medicines (Basel). 2017;4(2):42.
[21] Donkor AM, Kwofie SK, Darko G, Agyemang K. Evaluation of extracts from Sida acuta, *Phyllanthus amarus* and Parkia biglobosa for antimicrobial and antioxidant activities. BMC Complement Med Ther. 2023;23:289.
[22] Njideaka OT, Abdullahi M, Oche O. Antioxidant and phytochemical analysis of methanol extract of *Phyllanthus amarus*. FUDMA J Sci. 2024;8(3):2724.

[23] Adams RP. Identification of essential oil components by gas chromatography/mass spectrometry. 4th ed. Carol Stream: Allured Publishing; 2007.
[24] Chavan ND, Upadhyay KD. Quinoline derivatives' biological interest for anti-malarial and anti-cancer activities: an overview. RSC Adv. 2025;15(37):30576-30604.
[25] García MD, Sáenz MT, Gómez MA, Fernández MA. Topical anti-inflammatory activity of phytosterols isolated from Eryngium foetidum. Phytother Res. 2009;14(1):70-2.
[26] Sofowora A. Medicinal plants and traditional medicine in Africa. 3rd ed. Ibadan: Spectrum Books; 2008.
[27] Elmaidomy AH, Abdelmohsen UR, Sayed AM. Antiplasmodial potential of phytochemicals from Citrus aurantifolia peels: a comprehensive *in vitro* and *In silico* study. BMC Chem. 2024;18:60.
[28] Aliyu K, Umar A, Bello M, Abdullahi M. *In vitro* antiplasmodial activity of *Phyllanthus amarus* against *Plasmodium falciparum* and evaluation of its acute toxicity effect in mouse model. Trop Parasitol. 2021;11(1):26-33.
[29] Appiah-Opong R, Nyarko AK, Dodoo D, Gyang FN, Afriyie DK. Antiplasmodial activity of extracts of Tridax procumbens and *Phyllanthus amarus* in *in vitro Plasmodium falciparum* culture systems. Ghana Med J. 2011;45(4):143-50.
[30] Sanz LM, Crespo B, De-Cózar C, Ding XC, Llergo JL, Burrows JN, *et al*. *P. falciparum in vitro* killing rates allow to discriminate between different antimalarial mode-of-action. PLoS One. 2012;7(2):e30949.
[31] Chaianantakul N, Sirawaraporn R, Sirawaraporn W. Insights into the role of the junctional region of *Plasmodium falciparum* dihydrofolate reductase-thymidylate synthase. Malar J. 2013;12:91.
[32] Akinwumi AF, Faleti OE, Ogunleye AJ. *In silico* studies of bioactive compounds selected from four African plants with inhibitory activity against *Plasmodium falciparum* dihydrofolate reductase. Semantic Scholar [Internet]. 2023 [cited 2025 Apr 17]. Available from: https://www.semanticscholar.org
[33] McGinnis S, Madden TL. BLAST: at the core of a powerful and diverse set of sequence analysis tools. Nucleic Acids Res. 2004;32(Web Server issue):W20-5.
[34] Oktriawan T, Aulia BA, Setyawan T, Raharjo TJ, Haryadi W, Commeiras L, *et al*. Quinazolinone derivatives as targeting *Pf*DHFR and *Pf*DHODH inhibitor: *In silico* studies using molecular docking, molecular dynamics simulations, MM-PBSA, and ADMET analysis. Trends Sci. 2026;23(8):1331.
[35] Rasyid H. *In silico* design of isoindolinone-hydrazide hybrid compounds as antiplasmodium through molecular docking, molecular dynamics simulation, and MM-PBSA calculation. Curr Pharm Innov. 2026;120:990.
[36] Yusuf AJ, Alpha ARA, Salihu M, Aminu J, Yelekçi K, Imam MU. Integrated in vivo and *In silico* evaluation of antimalarial compounds from medicinal plants identified by GC-MS profiling. Front Drug Discov. 2025;5:1635697.

Acta Biomed 2026; Vol. 97, N. 1: ISSN: 0392-4203 | eISSN: 2531-6745

[37] Parr RG, Yang W. Density-functional theory of atoms and molecules. New York: Oxford University Press; 1989.
[38] Kutama AS, Bichi AH, Abdullahi G, Muhammad SS. Phytochemical screening and antimicrobial activities of *Phyllanthus amarus* extracts. Asian J Microbiol Biotechnol Environ Sci. 2022;24(2):357-65.